FULL PAPER

Multiple and Multipolar Fano Resonances in Plasmonic Nanoring Pentamers

Hailong Liu, Eunice Sok Ping Leong, Zilong Wang, Guangyuan Si, Longjiang Zheng, Yan Jun Liu,* and Cesare Soci*

The optical properties of plasmonic nanoring pentamers are experimentally and theoretically investigated in the near-infrared spectral region, where the nanoring metamolecules allow complex optical design by tuning a single geometrical parameter (the inner radius of the nanoring). Even in fully four-fold symmetric nanoring pentamers, unconventional plasmonic coupling paths generate multiple Fano resonances which would not appear in symmetric nanodisc oligomers. In addition, inhomogeneous elementary units in the pentamer induce additional resonances due to high-order dark modes, while complete breaking of the four-fold symmetry results in sharp multipolar Fano resonances upon the hybridization of dark and bright modes. This approach demonstrates a simple way to engineer plasmonic couplings by subtle changes of uniform metamaterial design.

1. Introduction

Plasmonic oligomers, close-packed nanoparticles with small gaps, have recently attracted intense attention for their analogy of atoms to build molecules in nanoscale size.[1,2] In the past few years, a variety of plasmonic oligomers as artificial plasmonic molecules, such as nanospheres,[3–7] nanoshells,[8,9] nanodisks,[10–31] nanotriangles,[32,33] nanorods,[34,35] and split-ring resonators,[36,37] have been demonstrated with unique optical properties (Fano resonance), hence enabling many potential applications in high-sensitivity biosensors,[4,9,11] photoelectric devices,[22,23] and surface-enhanced Raman scatterings.[14,17,27] These unique properties of the plasmonic oligomers are attributed to the plasmon couplings among their components. Usually, in symmetric plasmonic oligomers, there is only one plasmon coupling path, in which the dipole resonant mode of the central nanoparticle couples and hybridizes with the collective resonant behavior of the satellite nanoparticles to form a single Fano resonance.[38] Recently, plasmonic oligomers with multiple Fano resonances have been studied for their potential applications in multiwavelength biosensing and surface enhanced Raman scattering.[13,37] However, in such oligomers, the plasmon coupling path is still due to the central nanoparticle coupling with its peripheral satellites, and multiple Fano resonances are realized by tuning the collective behavior of the satellite particles.

Here we design, fabricate and characterize a new type of plasmonic oligomers, namely plasmonic nanoring pentamers (NRPs). Due to the unique optical properties of nanorings, the proposed oligomers are shown to support multiple plasmon coupling paths, which lead to multiple Fano resonances without breaking the underlying symmetry of the nanostructures. A geometrical design parameter, the ring width-to-radius ratio (RWTR), is proposed to predict and tune the number of Fano resonances of NRPs. Moreover, nanorings support more plasmonic resonant modes, which offer the freedom to engineer rich optical properties. By tuning the inner radius of the center nanoring (or center and side nanorings), sharp multipolar Fano resonances are demonstrated in this work. Additional optical features can also be realized by tuning the design of groups of constituent nanorings, which makes the proposed NRPs a new, flexible platform for the development of functional plasmonic molecules.

2. Results and Discussion

Plasmonic NRPs were fabricated on a quartz substrate by electron-beam lithography. Initially we considered a set of gold NRPs with different inner radii (r_{in}) and fixed outer radius (r_{out}). **Figure 1**(a) shows the SEM images of the fabricated symmetric NRP arrays with outer radii of 110 nm and inner radii of 80, 65, and 45 nm, respectively. For the sake of brevity, the

Dr. H. L. Liu, Prof. L. J. Zheng
Measurement Technology & Instrumentation
Key Lab of Hebei Province
Institute of Electrical Engineering
Yanshan University
Hebei, 066004, China
E-mail: liuhl@ysu.edu.cn
Dr. H. L. Liu, Z. L. Wang, Prof. C. Soci
Centre for Disruptive Photonic Technologies
Nanyang Technological University
21 Nanyang Link, 637371, Singapore
Dr. E. S. P. Leong, Dr. Y. J. Liu
Institute of Materials Research and Engineering
Agency for Science
Technology and Research (A*STAR)
3 Research Link, 117602, Singapore
E-mail: liuy@imre.a-star.edu.sg
Dr. G. Y. Si
College of Information Science and Engineering
Northeastern University
Shenyang, 110004, China

DOI: 10.1002/adom.201300393

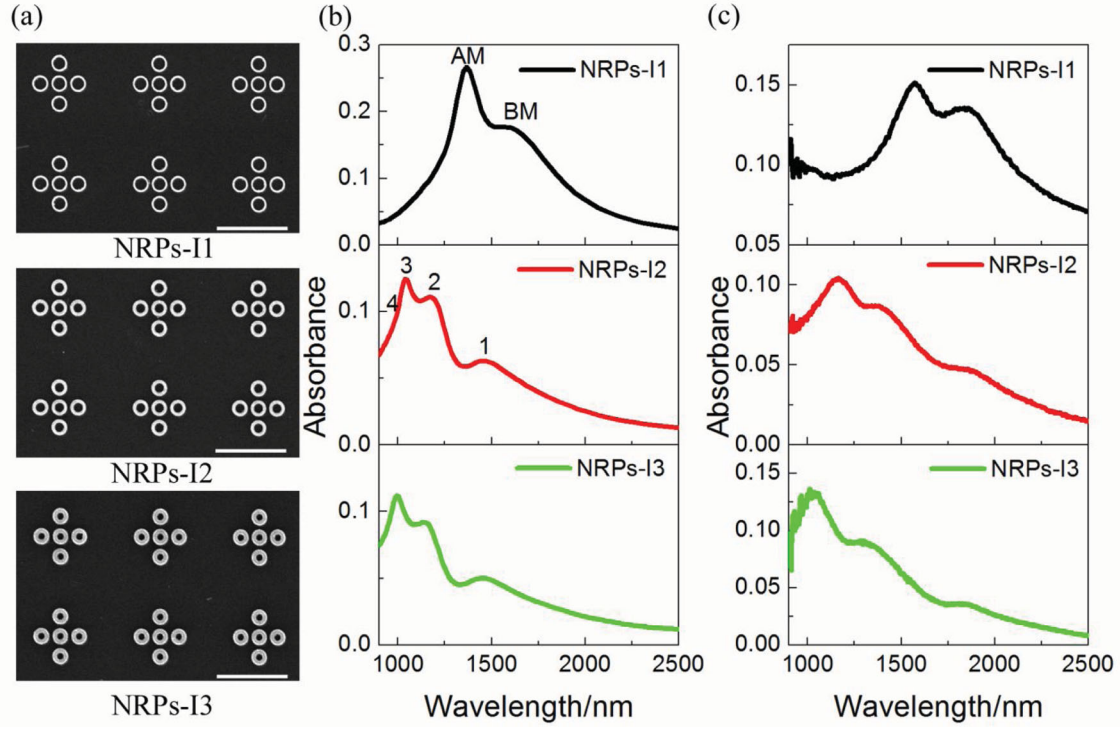

Figure 1. NRP arrays with gradually decreasing inner radii and corresponding absorbance spectra. a) SEM images of NRPs-I1 (top, r_{in} = 80 nm), NRPs-I2 (middle, r_{in} = 65 nm), and NRPs-I3 (bottom, r_{in} = 45 nm). Scale bar: 1 μm. Simulated (b) and measured (c) absorbance spectra of NRPs-I1, NRPs-I2, and NRPs-I3.

NRP arrays from larger to smaller inner radii will be termed as NRPs-I1, NRPs-I2, and NRPs-I3. Figure 1(b),(c) illustrate finite-difference time-domain simulations and measured absorbance spectra for these NRP arrays. Here, the measured absorbance spectrum of NRPs is defined as log_{10}(1/Transmission). Overall, the spectral profiles of simulations and experiments are in good agreement. Compared to the simulation results, the experimental absorbance peaks are slightly red-shifted, which could be mainly attributed to the shape tolerance and refractive index differences between simulations and experiments.

In the case of NRPs-I1, two clear peaks (marked by AM and BM) are observed in both simulated and experimental spectra. To reveal their nature, the near-field charge and electric-field distributions at these two peaks are calculated (see Figure S1 in supporting information). According to the plasmon hybridization model, the optical spectra of complex plasmonic molecules can be decomposed into the plasmon couplings among simple plasmonic atoms.[39,40] The charge distributions in Figure S1 show that the AM and BM peaks of NRPs-I1 can be decomposed into the plasmon couplings between the three vertical nanorings (subgroup A) and the left and right nanorings (subgroup B). Plasmons of subgroups A and B couple and hybridize to form a bonding mode (BM) and an antibonding mode (AM), in which the two subgroups are out-of-phase and in-phase, respectively. They overlap and lead to a destructive interference, which give rise to a dipolar Fano resonance.

The ring width-to-radius ratio of NRPs-I1 is RWTR = 0.27. Interestingly, increasing the RWTR of each nanoring in symmetric NRPs results in the appearance of additional plasmonic resonance peaks that correspond to more complex plasmon coupling paths. This is shown for NRPs-I2 and NRPs-I3 in Figure 1. In NRPs-I2, the inner radius is 65 nm (RWTR = 0.41), and three plasmonic resonance peaks are observed (marked by 1, 2, and 3). As the inner radius further decreases to 45 nm in NRPs-I3, (RWTR = 0.59), these three peaks are blue-shifted with respect to those of NRPs-I2. The corresponding charge and electric-field distributions for peaks 1, 2, and 3 are calculated to reveal the plasmon coupling paths (**Figure 2**). For peak 1, the charges of the three vertical nanorings (subgroup I) and the left and right nanorings (subgroup II) are out-of-phase, as shown in Figure 2(a). Therefore, the plasmon coupling path for peak 1 results from a bonding mode (dark mode) between subgroup I and II, similar to the case of peak BM in NRPs-I1 (Figure S1). More importantly, charge and electric-field distributions of peaks 2 and 3 in Figure 2(b) and (c) present two new plasmon coupling paths. For peak 2, the two coupling subgroups are the three transverse nanorings (subgroup III) and the top and bottom nanorings (subgroup IV). For peak 3, the two subgroups are the four satellite nanorings (subgroup V) and the center nanoring (subgroup VI). For both peaks, the charges of the subgroups are still out-of-phase, therefore, peaks 2 and 3 are dark modes. As a result, three dark modes (corresponding to three plasmon coupling paths) are observed in the absorbance spectra of NRPs-I2. According to the plasmon hybridization model, the charge distributions of the bright mode corresponding to each dark mode in NRPs-I2 should have in-phase charge profiles between the two hybridized subgroups. Interestingly, we found that the bright modes corresponding to

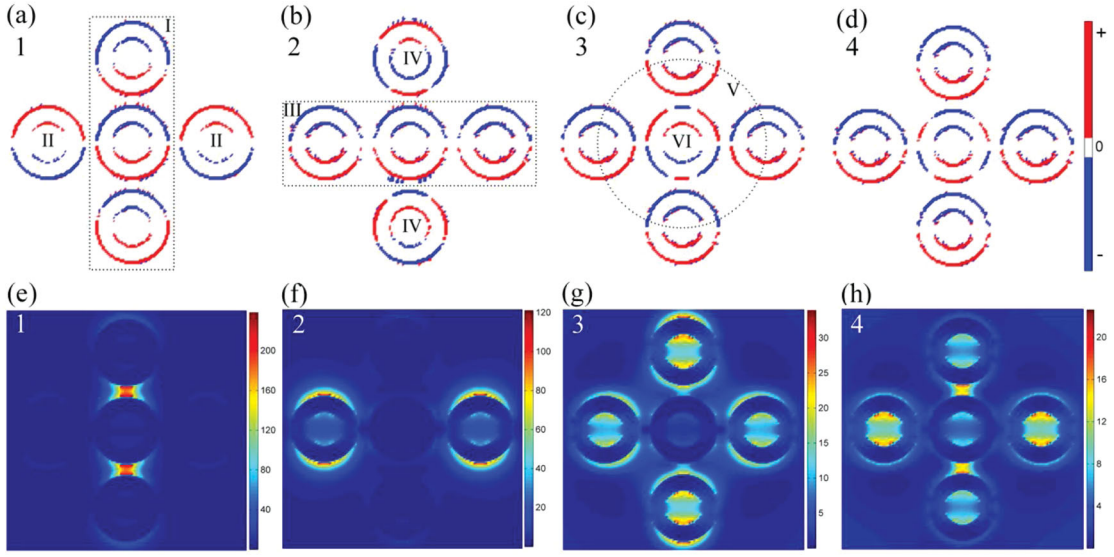

Figure 2. Near-field charge and electric-field distributions for different resonant wavelengths in NPR-I2: peak 1 (a) and (e), peak 2 (b) and (f), peak 3 (c) and (g), position 4 (wavelength of 980 nm) (d) and (f). The up row displays the charge distributions, and the bottom row illustrates the electric-field distributions.

dark modes 1, 2, and 3 have the same charge configurations, in which all the five nanorings oscillate in-phase. Figure 2(d) shows that the charge distributions in all the five nanorings are in-phase for spectral position 4 (wavelength of 980 nm), and thus the net sum of their dipole moments is increased. Consequently, mode 4 is an antibonding, superradiant, and bright mode. The dark modes overlap and destruct the bright mode, leading to multiple Fano resonances.

To further understand the origin of the additional plasmon coupling paths in NRPs-I2, we decomposed the optical spectra of NRPs into the spectra plasmon coupling between two subgroups by multilayer plasmon hybridization model.[39,40] The couplings between subgroups III and IV for NRPs-I2 are given in **Figure 3**. In Figure 3(a), the two peaks marked as TA and TB in the optical spectra for subgroup III and the corresponding charge distributions show that they correspond to antibonding and bonding modes between the center nanoring and the left and right nanorings. In Figure 3(c), there is only one resonant peak for the upper and lower nanorings (subgroup IV), and the corresponding charge discovers the dipole and bright nature. The antibonding mode (TA) of subgroup III and the dipole mode of subgroup IV couple and hybridize to form a dark mode (peak 2) and a bright mode (4) in NRPs-I2, shown in Figure 3(b). The case of peak 3 is similar to peak 2. For comparison, the corresponding peaks (2 and 3) can not be observed in NRPs-I1. The corresponding hybridization process for NRPs-I1 is presented to explore this reason, as shown in Figure S2. The RWTR of NRPs-I1 is 0.27, which makes the coupling strength of the antibonding mode of the three transverse nanorings very weak (see the green dot in Figure S2(a)). Consequently, the coupling path between the antibonding mode of three transverse nanorings and the bright mode of the upper and lower nanorings in NRPs-I1 is unfavorable and cannot be observed. Compared to NRPs-I2, the blue-shift of the peaks in NRPs-I3 can be explained by the blue-shift of the corresponding resonances of the subgroups owing to the increasing RWTR. This analysis shows that, based on the plasmon hybridization model, one can tune the plasmon coupling pathways in plasmonic NRPs by simply varying the RWTR, which then provides a flexible platform for the design and development of a variety of functional plasmonic molecules with common underlying geometry.

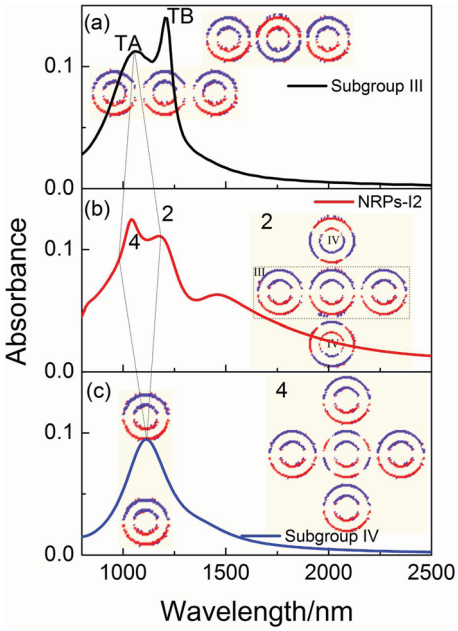

Figure 3. Plasmon couplings between subgroups III and IV in NRPs-I2. Absorbance spectrum and corresponding charge distributions of subgroup III (a), NRPs-I2 (b), and subgroup IV (c).

Figure 4 displays the effect of varying the inner radius of the central nanoring on the optical properties of NRPs. Compared

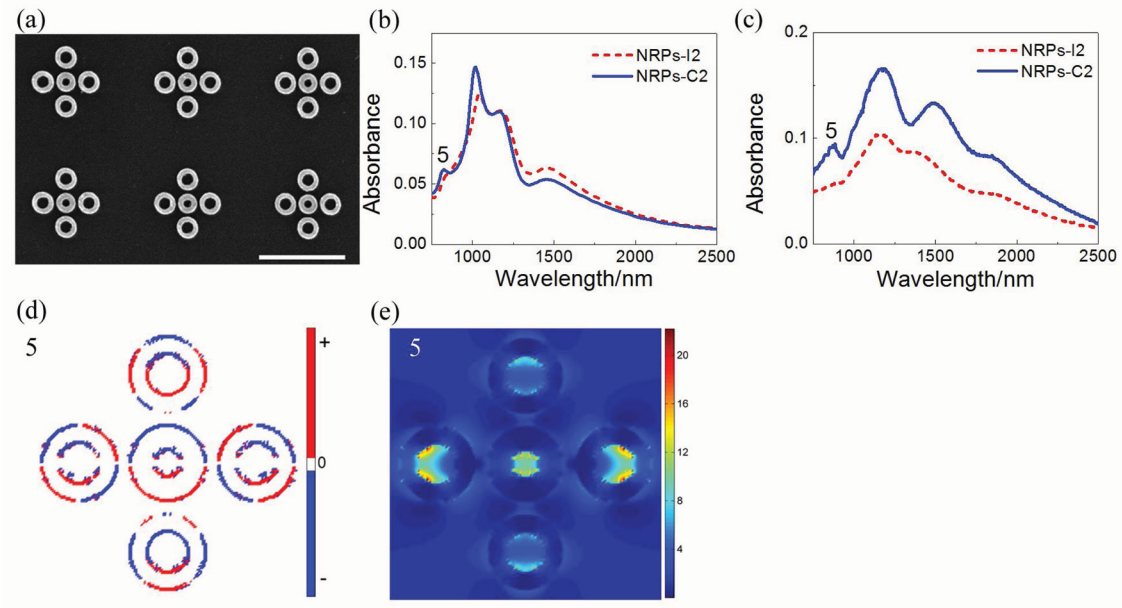

Figure 4. Optical properties of NRPs-C2. a) SEM image of NRPs-C2. Scale bar: 1 μm. Simulated (b) and measured (c) absorbance spectra of NRPs-C2. Charge (d) and electric-field (e) distributions of peak 5.

to NRPs-I2 in Figure 1, the inner radius of the central nanoring was decreased from 65 to 45 nm, without breaking the four-fold symmetry of the structure. For simplicity, the NRP array in Figure 4(a) is termed NRPs-C2. Figure 4(b) and (c) show the comparison between simulated and measured absorbance spectra of NRPs-C2 and NPRs-I2. Notably, a new peak appears at 880 nm in NRPs-C2, labeled as peak 5 in Figure 4(c). This feature is clearly observed also in the simulations shown in Figure 4(b). From the corresponding charge distributions in Figure 4(d) it is seen that the upper and lower nanorings (subgroup IV) oscillate in quadrupolar modes, while the three transverse nanorings (subgroup III) form a bright dipolar mode. These two subgroups eventually couple and hybridize to form a quadrupole-dipole resonant mode. Based on the phase of the charge, we conclude that the coupled quadrupole-dipole mode is a dark mode. With respect to NRPs-I2, the inner radius of the center nanoring is decreased in NRPs-C2, thus the resonant energy of the bright mode between the center nanoring and the left and right nanorings increases to approach the quadrupolar resonant energy of the upper and lower nanorings. Therefore, these modes can couple and hybridize to form a quadrupole-dipole plasmonic dark mode, which due to the overlap with the bright mode forms a third Fano resonance.

When the symmetry of the NRPs is broken by tuning the inner radii of satellite nanorings, much richer spectral features and additional Fano resonances can be observed. **Figure 5**(a) shows the SEM image of an asymmetric NRP array, termed as NRPs-CR. The inner radii of the central and right nanorings are 45 and 65 nm, while other parameters are the same as those of NRPs-I1 in Figure 1(a). Both simulated and experimental absorbance spectra for NRPs-CR are shown in Figure 5(b) and (c). Five peaks are observed in the simulation spectra (A to D), while peaks B and C merge into a single broad peak in experimental spectra. This may be due to inhomogeneous broadening in nonperfectly uniform patterns. Compared to Figure 1, the smaller inner radii of the central and rightmost nanorings induce an obvious spectral change. The plasmon coupling paths corresponding to peaks D and E are characterized by the corresponding charge and electric-field distributions in Figure 5(d) and (e). Interestingly, two quadrupolar plasmon resonant modes (modes D and E) are presented in NRP-CR. The charge distributions at spectral positions D and E show that the upper and lower nanorings oscillate in quadrupolar modes, while the other three nanorings in dipolar modes. The quadrupolar modes of upper and lower nanorings hybridize with the dipolar modes of the three transverse nanorings to form an antibonding quadrupole-dipole mode and a bonding quadrupole-dipole mode (D and E). The destructive interference between the bright mode (D) and dark mode (E) gives rise to quadrupolar-quadrupolar Fano resonance. It has been theoretically and experimentally proved that multipolar (quadrupolar, octupolar, etc.) Fano resonances in nanostructures such as "XI" nanostructures,[41] theta-shaped nanoparticles,[42] and ring/disk nanostructures,[43–45] etc. have lower radiative losses, sharper peaks, and higher sensitivities to refractive index change than dipolar Fano resonances.[46] Hence, realization of multipolar Fano resonances in plasmonic oligomers may be highly beneficial to achieve high sensitivity in plasmonic biosensors.

The plasmon coupling paths for peaks A, B and C are shown in Figure S3. According to their charge distributions, we conclude that peaks A and C are dark modes, similar to the plasmon coupling paths of peaks 1 and 3 in NRPs-I2. The plasmon coupling path for mode B in NRPs-CR, however, is complex and differs from mode 2 in NRPs-I2. The reason for the difference is the decreased inner radii of the center and rightmost nanorings change the configurations of the dipole momentum of the nanorings. In mode B of NRPs-CR, one subgroup consists of the four leftmost nanorings oscillating in opposition of phase

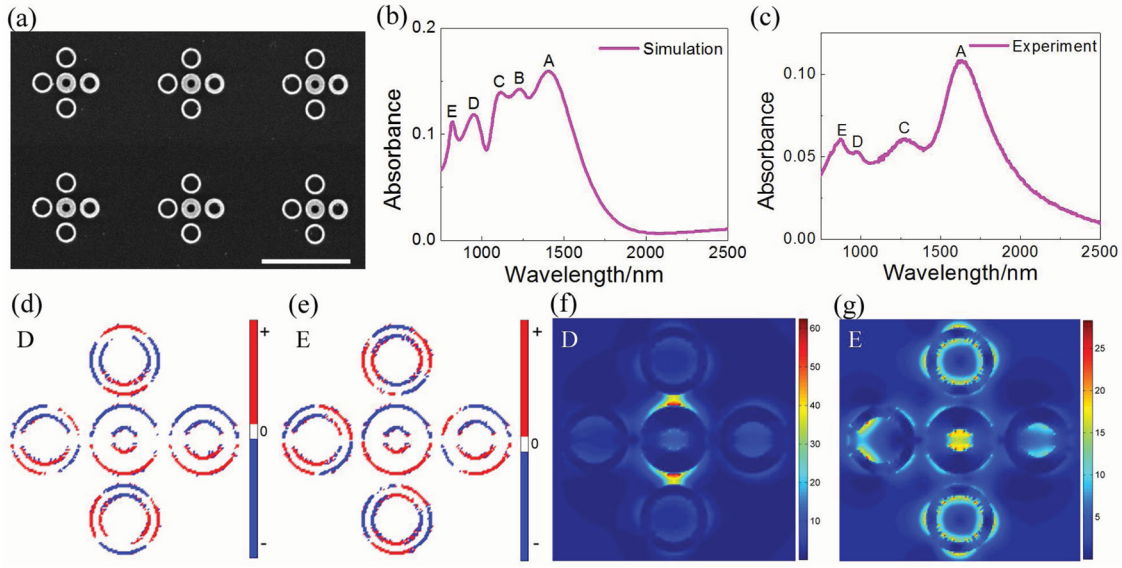

Figure 5. Optical properties of NRPs-CR. (a) SEM image of NRPs-CR. Scale bar: 1 μm. Simulated (b) and measured (c) absorbance spectra of NRPs-CR. Charge distributions (d) and electric-field distributions (e) corresponding to spectral positions A, B, C, D, and E in the absorbance spectrum of NRPs-CR.

with respect to the other subgroup consisting of the rightmost nanoring only. This shows that even more complex plasmon coupling paths and high-order Fano resonance are achievable when breaking the symmetry of NRPs.

3. Conclusion

We investigated the optical properties of plasmonic nanoring pentamers both theoretically and experimentally. Fano resonances are easily tuned by varying the inner radii of nanorings, while keeping the fully four-fold symmetry unchanged. Multiple Fano resonances were demonstrated for the first time in symmetric plasmonic nanoring pentamers. By breaking the symmetry of plasmonic nanoring pentamers, more complex plasmon coupling paths and high-order Fano resonance are also demonstrated. Tunability of the Fano resonances in the various structures can be understood with a multiple-layer plasmon hybridization model. The specific features of plasmonic nanoring oligomers make them a good "universal" platform for designing and developing plasmonic molecules with desired functions, which may find applications in biosensing, surface-enhanced Raman scattering, and optical filters.

4. Experimental Section

Plasmonic NRPs were fabricated on a quartz substrate using electron-beam lithography followed by metal evaporation and lift-off. A set of gold NRPs were fabricated with inner radius, r_{in}, varying from 80 nm to 45 nm and fixed outer radius of r_{out} = 110 nm. The gap between central and satellite nanorings was 40 nm. The periodicities of all the arrays were fixed at 1.4 μm. The patterned area of each NRP array was 30 × 30 μm^2. The thickness of gold nanorings was 30 nm. Before gold deposition, a thin layer of titanium (3 nm) was evaporated to enhance the adhesion of gold nanorings onto the quartz substrate. The near infrared absorbance spectra of NRPs were obtained by combining measurements with a Fourier-transform infrared spectrometer (FTIR: Bruker Vertex 80) equipped with a confocal microscope and a UV-vis-NIR microspectrophotometer (CRAIC QDI 2010). Both optical spectra and corresponding near-field distributions of NRPs were modeled using the finite-difference time-domain method.

Supporting Information

Supporting Information is available from the Wiley Online Library or from the author.

Acknowledgements

Dr. H. L. Liu and Dr. E. S. P. Leong contributed equally to this work. This work is partially supported by the National Natural Science Foundation of China (Grant No. 61007005), the Natural Science Foundation of Hebei Province (Grant No. F2011203022), the Foundation of Department of Education of Hebei Province (Grant No. Y2012030), the NTU-NAP startup grant No. M4080511, and the Ministry of Education of Singapore (Grant No. MOE2011-T3–1–005). E.S.P. Leong and Y.J. Liu also thank the funding support from Joint Council Office (JCO) of the Agency for Science, Technology and Research (A*STAR) under the grant No. 12302FG012.

Received: September 22, 2013
Revised: October 12, 2013
Published online: October 30, 2013

[1] J. A. Fan, C. Wu, K. Bao, J. Bao, R. Bardhan, N. J. Halas, V. N. Manoharan, P. Nordlander, G. Shvets, F. Capasso, *Science* **2010**, *328*, 1135.
[2] M. Hentschel, M. Saliba, R. Vogelgesang, H. Giessen, A. P. Alivisatos, N. Liu, *Nano Lett.* **2010**, *10*, 2721.
[3] D. W. Brandl, N. A. Mirin, P. Nordlander, *J. Phys. Chem. B* **2006**, *110*, 12302.

[4] N. A. Mirin, K. Bao, P. Nordlander, *J. Phys. Chem. A* **2009**, *113*, 4028.
[5] K. Bao, N. A. Mirin, P. Nordlander, *Appl. Phys. A—Mater. Sci. Process* **2010**, *100*, 333.
[6] L. Chuntonov, G. Haran, *Nano Lett.* **2011**, *11*, 2440.
[7] S. N. Sheikholeslami, A. Garcia-Etxarri, J. A. Dionne, *Nano Lett.* **2011**, *11*, 3927.
[8] J. A. Fan, K. Bao, C. Wu, J. Bao, R. Bardhan, N. J. Halas, V. N. Manoharan, G. Shvets, P. Nordlander, F. Capasso, *Nano Lett.* **2010**, *10*, 4680.
[9] J. A. Fan, Y. He, K. Bao, C. Wu, J. Bao, N. B. Schade, V. N. Manoharan, G. Shvets, P. Nordlander, D. R. Liu, F. Capasso, *Nano Lett.* **2011**, *11*, 4859.
[10] J. Alegret, T. Rindzevicius, T. Pakizeh, Y. Alaverdyan, L. Gunnarsson, M. Kall, *J. Phys. Chem. C* **2008**, *112*, 14313.
[11] J. B. Lassiter, H. Sobhani, J. A. Fan, J. Kundu, F. Capasso, P. Nordlander, N. J. Halas, *Nano Lett.* **2010**, *10*, 3184.
[12] M. Hentschel, D. Dregely, R. Vogelgesang, H. Giessen, N. Liu, *ACS Nano* **2011**, *5*, 2042.
[13] D. Dregely, M. Hentschel, H. Giessen, *ACS Nano* **2011**, *5*, 8202.
[14] A. J. Pasquale, B. M. Reinhard, L. D. Negro, *ACS Nano* **2011**, *5*, 6578.
[15] P. Alonso-Gonzalez, M. Schnell, P. Sarriugarte, H. Sobhani, C. Wu, N. Arju, A. Khanikaev, F. Golmar, P. Albella, L. Arzubiaga, F. Casanova, L. E. Hueso, P. Nordlander, G. Shvets, R. Hillenbrand, *Nano Lett.* **2011**, *11*, 3922.
[16] J. B. Lassiter, H. Sobhani, M. W. Knight, W. S. Mielczarek, P. Nordlander, N. J. Halas, *Nano Lett.* **2012**, *12*, 1058.
[17] J. Ye, F. Wen, H. Sobhani, J. B. Lassiter, P. V. Dorpe, P. Nordlander, N. J. Halas, *Nano Lett.* **2012**, *12*, 1660.
[18] F. Wen, J. Ye, N. Liu, P. V. Dorpe, P. Nordlander, N. J. Halas, *Nano Lett.* **2012**, *12*, 5020.
[19] N. Liu, S. Mukherjee, K. Bao, Y. Li, L. V. Brown, P. Nordlander, N. J. Halas, *ACS Nano* **2012**, *6*, 5482.
[20] N. Liu, S. Mukherjee, K. Bao, L. V. Brown, J. Dorfmüller, P. Nordlander, N. J. Halas, *Nano Lett.* **2012**, *12*, 364.
[21] W. S. Chang, J. B. Lassiter, P. Swanglap, H. Sobhani, S. Khatua, P. Nordlander, N. J. Halas, S. Link, *Nano Lett.* **2012**, *12*, 4977.
[22] Z. Fang, Z. Liu, Y. Wang, P. M. Ajayan, P. Nordlander, N. J. Halas, *Nano Lett.* **2012**, *12*, 3808.
[23] Z. Fang, Y. Wang, Z. Liu, A. Schlather, P. M. Ajayan, F. H. L. Koppens, P. Nordlander, N. J. Halas, *ACS Nano* **2012**, *6*, 10222.
[24] M. Hentschel, M. Schaferling, T. Weiss, N. Liu, H. Giessen, *Nano Lett.* **2012**, *12*, 2542.
[25] M. Hentschel, L. Wu, M. Schaferling, P. Bai, E. P. Li, H. Giessen, *ACS Nano* **2012**, *6*, 10355.
[26] Y. Cui, J. Zhou, V. A. Tamma, W. Park, *ACS Nano* **2012**, *6*, 2385.
[27] A. J. Pasquale, B. M. Reinhard, L. D. Negro, *ACS Nano* **2012**, *6*, 4341.
[28] M. Rahmani, D. Y. Lei, V. Giannini, B. Luk'yanchuk, M. Ranjbar, T. Y. F. Liew, M. Hong, S. A. Maier, *Nano Lett.* **2012**, *12*, 2101.
[29] M. Rahmani, B. Luk'yanchuk, T. T. V. Nguyen, T. Tahmasebi, Y. Lin, T. Y. F. Liew, M. H. Hong, *Opt. Mater. Express* **2010**, *1*, 1409.
[30] M. Rahmani, B. Luk'yanchuk, B. Ng, K. G. A. Tavakkoli, Y. F. Liew, M. H. Hong, *Opt. Express* **2011**, *19*, 4949.
[31] J. Yang, M. Rahmani, J. H. Teng, M. H. Hong, *Opt. Mater. Express* **2012**, *2*, 1407.
[32] A. L. Koh, A. I. Fernandez-Dominguez, D. W. McComb, S. A. Maier, J. K. W. Yang, *Nano Lett.* **2011**, *11*, 1323.
[33] J. Zhao, B. Frank, S. Burger, H. Giessen, *ACS Nano* **2011**, *5*, 9009.
[34] A. Artar, A. A. Yanik, H. Altug, *Nano Lett.* **2011**, *11*, 3694.
[35] R. Taubert, M. Hentschel, J. Kastel, H. Giessen, *Nano Lett.* **2012**, *12*, 1367.
[36] A. W. Clark, J. M. Cooper, *Adv. Mater.* **2010**, *22*, 4025.
[37] S. D. Liu, Z. Yang, R. P. Liu, X. Y. Li, *ACS Nano* **2012**, *6*, 6260.
[38] M. Rahmani, B. Luk'yanchuk, M. Hong, *Laser Photon. Rev.* **2013**, *7*, 329.
[39] E. Prodan, C. Radloff, N. J. Halas, P. Nordlander, *Science* **2003**, *302*, 419.
[40] H. Liu, X. Wu, B. Li, C. Xu, G. Zhang, L. Zheng, *Appl. Phys. Lett.* **2012**, *100*, 153114.
[41] N. Verellen, P. V. Dorpe, C. Huang, K. Lodewijks, G. A. E. Vandenbosch, L. Lagae, V. V. Moshchalkov, *Nano Lett.* **2011**, *11*, 391.
[42] T. G. Habteyes, S. Dhuey, S. Cabrini, P. J. Schuck, S. R. Leone, *Nano Lett.* **2011**, *11*, 1819.
[43] F. Hao, P. Nordlander, Y. Sonnefraud, P. V. Dorpe, S. A. Maier, *ACS Nano* **2009**, *3*, 643.
[44] Y. Zhang, T. Jia, H. Zhang, Z. Xu, *Opt. Lett.* **2012**, *37*, 4919.
[45] A. E. Cetin, H. Altug, *ACS Nano* **2012**, *6*, 9989.
[46] B. Luk'yanchuk, N. I. Zheludev, S. A. Maier, N. J. Halas, P. Nordlander, H. Giessen, C. T. Chong, *Nat. Mater.* **2010**, *9*, 707.